PNAS RESEARCH ARTICLE | PHYSIOLOGY

Endothelial Arf6 sustains electrical signaling and cerebral blood flow in mice through PIP_2-dependent activation of Kir2.1 channels

Maria F. Noterman-Soulinthavong[a], María Sancho[a,b], Saúl Huerta de la Cruz[a], Michael Yarboro[a], Maurizio Mandalà[a,c], Masayo Koide[a], Nathalie Beaufort[d], Katalin Todorov-Völgyi[d], Emma Moreland[a], David Hill-Eubanks[a], Martin Dichgans[d,e,f,g], and Mark T. Nelson[a,h,1]

Affiliations are included on p. 9.

Contributed by Mark T. Nelson; received April 28, 2026; accepted June 8, 2026; reviewed by Madeline Nieves-Cintron and Ravi L. Rungta

Brain capillaries sense neural activity and direct blood flow to active regions—a process termed neurovascular coupling that underlies activity-dependent increases in local perfusion (functional hyperemia). A key contributor to functional hyperemic responses is the capillary endothelial cell (cEC) inward rectifier K^+ (Kir2.1) channel, which, when activated by neuronal activity–derived extracellular K^+, initiates vasodilatory electrical signals that propagate through the vascular network. Kir2.1 channel function requires continual production of its lipid cofactor, phosphatidylinositol-4,5-bisphosphate (PIP_2), and is compromised in mouse models of cerebral small vessel (cSVD). Although decreased PIP_2 availability is a common feature of cSVDs, mechanisms underlying PIP_2 synthesis remain poorly understood. We hypothesized that Arf6, a small GTPase expressed in cECs that stimulates PIP_2 production, is critical for this process. Using patch-clamp electrophysiology, we demonstrate that inhibiting Arf6 activity progressively decreased cEC Kir2.1 channel activity. This deficit manifested as loss of capillary-to-arteriole electrical signaling in isolated vessels and diminished functional hyperemia in vivo. Exogenously provided PIP_2 restored Kir2.1 currents and functional hyperemia after Arf6 inhibition or genetic knockdown. Collectively, our data suggest that cEC Arf6 sustains Kir2.1 activity by maintaining PIP_2 levels and demonstrate that diminished PIP_2 synthesis is sufficient to impair functional hyperemia. Furthermore, we identify Arf6 as a mechanistic link between PIP_2 production and endothelial electrical signaling, highlighting Arf6 as a potential therapeutic target for restoring functional hyperemia.

cerebral blood flow | endothelial cells | ADP-ribosylation factor 6 | Kir2.1 channels | phosphatidylinositol-4,5-bisphosphate

Significance

Active brain regions send electrical signals through capillaries that dilate upstream arterioles and increase blood flow. The resulting activity-dependent increase in local blood flow (functional hyperemia) is mediated by inward-rectifier potassium (Kir2.1) channels. These channels require continuous regeneration of the lipid cofactor PIP_2 (phosphatidylinositol-4,5-bisphosphate). If PIP_2 is deficient, electrical signaling and functional hyperemia are impaired, defects characteristic of cerebral small vessel disease and Alzheimer's disease models. Here, we identify the small GTPase Arf6 as a key to maintaining PIP_2 synthesis and thus preserving capillary Kir2.1 activity and functional hyperemia. Our findings reveal an important pathway for PIP_2 homeostasis and position Arf6 as a cornerstone upholding functional hyperemic responses, highlighting Arf6 as a target for restoring cerebral blood flow in disease.

The capillary network comprises the smallest and most abundant vessels in the brain vasculature and serves as the nexus for nutrient and O_2 exchange. Beyond these passive functions, capillaries play a key role in neurovascular coupling, as they can detect neuronal activity and initiate hyperemic responses, thus acting as a "sensory web" that links local increases in neuronal activity with increased perfusion (functional hyperemia) (1–4). While multiple known mechanisms facilitate functional hyperemia, a striking ~60% of this response reflects electrical signaling mediated by capillary endothelial cells (cECs) through strong inwardly rectifying Kir2.1 potassium (K^+) channels (2, 5–7). Kir2.1 channels exhibit dual activation by extracellular K^+ and hyperpolarization, biophysical properties that enable these channels to translate physiological K^+ released during neuronal repolarization into vascular electrical signals and support far-reaching signal transmission through regenerative hyperpolarization between electrically coupled cECs (2, 8, 9). Thus, the cEC Kir2.1 channel governs the neuronal activity–triggered hyperpolarization that travels from capillaries to arterioles, where it relaxes smooth muscle cells (SMCs) and dilates arterioles, ultimately increasing cerebral blood flow (CBF) to the site of signal initiation (2, 3, 10–12).

Kir2.1 activity requires binding of its obligate cofactor, phosphatidylinositol-4,5-bisphosphate (PIP_2)—a plasma membrane phospholipid that regulates endocytosis, exocytosis, and numerous ion channel functions (2, 13–16). Similar to the case for other second messengers, PIP_2 pools are small, constituting <1% of total phospholipids, and highly dynamic, turning over every 20 to 180 s in unstimulated cells (17, 18). This dynamic aspect of PIP_2 availability is determined by its metabolism. Phosphorylation of PIP_2 to PIP_3 by phosphoinositide 3-kinase (PI3K) or hydrolysis to IP_3 and diacylglycerol by phospholipase C (PLC) depletes PIP_2, deactivating ion channels that require it, including Kir2.1 channels (15, 19). Counteracting these depletion mechanisms are lipid kinases that synthesize PIP_2, primarily

Reviewers: M.N.-C., University of California Davis; and R.L.R., Universite de Montreal.

The authors declare no competing interest.

[1]To whom correspondence may be addressed. Email: Mark.Nelson@uvm.edu.

This article contains supporting information online at https://www.pnas.org/lookup/suppl/doi:10.1073/pnas.2615120123/-/DCSupplemental.

Published July 7, 2026.

through sequential phosphorylation of phosphatidylinositol (PI) by phosphatidylinositol-4-kinase (PI4K) and phosphatidylinositol-4-phosphate (PIP) by type I phosphatidylinositol-4-phosphate 5-kinase I (PIP5KI) (Fig. 1*A*) (15). Unimpeded, the enzymes PI4K and PIP5KI can adaptively increase intracellular PIP_2 synthesis by up to 40-fold and 500-fold, respectively—a remarkable homeostatic feedback mechanism termed "regeneration" by the Hille group (15).

We have shown that inhibiting either PI4K or PIP5KI rapidly impairs Kir2.1 channel activity, suggesting that ongoing PIP_2 synthesis is essential for sustained Kir2.1 channel function (19). Furthermore, pathological mechanisms that decrease PIP_2 synthesis or increase its consumption have been implicated in mouse models of cerebral small vessel disease (cSVD)—the leading cause of vascular dementia (7, 20, 21). Strikingly, increasing PIP_2 availability normalizes functional hyperemia in all of these mouse models. Considering the prevalence of vascular dementia and the therapeutic challenge posed by diverse cSVD subtypes, these findings present the appealing concept that multiple cSVD disease mechanisms converge on a common pathway: PIP_2 metabolism (22). However, the molecular processes governing PIP_2 regeneration remain largely unknown (15).

To address this gap, we sought to identify candidate EC proteins that regulate PIP_2 synthesis and functional hyperemia. We focused on ADP-ribosylation factor 6 (Arf6), a small GTPase that cycles between GTP- and GDP-bound states, a dynamic regulated by the actions of guanine nucleotide exchange factors (GEFs) and GTPase-activating proteins (GAPs) (23–25). In its GTP-bound form, Arf6 stimulates PIP_2 synthesis by enhancing PIP5KI activity at the plasma membrane (Fig. 1*A*) (26–29). Intriguingly, there is also evidence that Arf6 expression in the cerebrovasculature decreases with age and in CADASIL (Cerebral Autosomal Dominant Arteriopathy with Subcortical Infarcts and Leukoencephalopathy), the most common monogenic cSVD (30, 31). Yet, while Arf6-mediated PIP_2 production and PIP_2-dependent Kir2.1 channel activity are independently well-established, the physiological relationship between Arf6 and Kir2.1 channel activity remains largely uninvestigated. Here, using pharmacological and genetic disruption of Arf6, we demonstrate that Arf6 sustains functional hyperemic responses by supporting the continuing synthesis of PIP_2 necessary to maintain EC Kir2.1 channel activity.

Results

Endothelial Arf6-Stimulated PIP_2 Production Sustains Kir2.1 Channel Activity. Arf6 has many identified roles in ECs (32–36), and its primary target, PIP5KI, is expressed in brain cECs as isoforms A–C, all of which share a highly conserved kinase core domain that binds Arf6 (29, 37, 38). To investigate a direct connection between Arf6 and PIP5KI activity in cECs, we used an ATP-depletion, kinase-activity assay to measure PIP5KI activity in microvessels from wild-type C57Bl/6J mouse brains (39). These well-described microvessel preparations, referred to hereafter as capillaries, are predominantly <10 μm in diameter, contain cECs, distal pericytes, and astrocytic endfeet (30, 39), but are largely devoid of contractile mural cells (determined by loss of an alpha smooth muscle actin-driven reporter) (Fig. 1*B*).

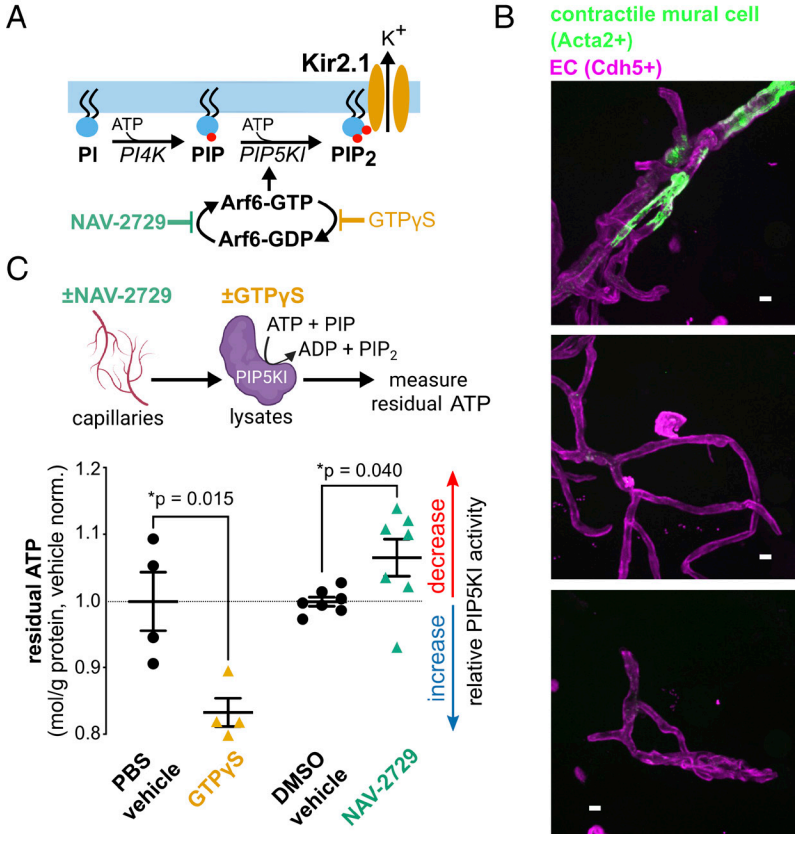

Fig. 1. Arf6 regulates PIP5KI activity in brain capillaries. (*A*) Schematic of the predominant pathway for synthesis of PIP_2 and the proposed regulatory role of Arf6 in brain cECs. NAV-2729 blocks GTP-GDP exchange, promoting the inactive Arf6-GDP form, whereas nonhydrolyzable GTPγS promotes active Arf6-GTP. (*B*) Fluorescence images from mice expressing genetically encoded fluorescent Ca^{2+} indicators in contractile mural cells (green, Acta2 promoter) and ECs (magenta, Cdh5 promoter). (Scale bar, 20 μm.) (*C*) PIP5KI activity, determined by adding equal amounts of ATP to capillary lysates acutely treated with 0.1 mM GTPγS (or vehicle controls) or 3 μM NAV-2729 (or vehicle controls). Data are normalized to vehicle average per batch (one batch for GTPγS and two for NAV-2729 comparisons) and are presented as means ± SEM [N = 4 to 7 male C57Bl/6J mice (3 to 4 mo old); GTPγS comparison by the unpaired *t* test: t(6) = 3.396; NAV-2729 comparison by the unpaired *t* test: t(12) = 2.302].

Lysates from capillaries treated with NAV-2729 (3 μM)—a small-molecule inhibitor of Arf6-GTP—or vehicle control (0.012% DMSO) were tested for endogenous PIP5KI enzymatic activity by incubating with PIP and ATP (40). In independent experiments, nonhydrolyzable GTPγS (0.1 mM) or its vehicle control [phosphate buffered saline (PBS)] was added to vessel lysates together with PIP and ATP (40). Residual ATP at the end of these incubations was measured as the inverse readout of pan-PIP5KI activity such that greater ATP depletion corresponds to higher PIP5KI activity. GTPγS treatment significantly increased capillary ATP consumption relative to PBS controls, indicating increased PIP5KI activity in the presence of active Arf6-GTP (Fig. 1*C*). Conversely, treatment with NAV-2729 significantly decreased ATP consumption by PIP5KI relative to dimethyl sulfoxide (DMSO) vehicle controls. Together, these findings indicate that capillary PIP5KI activity in isolated capillaries is sensitive to modulation of Arf6 activity.

We next tested whether Arf6 regulates cEC Kir2.1 channels through PIP_2, which is required for Kir2.1 channel function (19). To this end, we recorded currents from freshly isolated native brain cECs from wild-type mice in the conventional whole-cell configuration in response to 400-ms voltage ramps from −140 to +40 mV (holding potential: −50 mV) using our previously described methods (Fig. 2*A*) (2). Inward currents through Kir2.1 channels were elevated by raising extracellular $[K^+]_o$ in the bath to 60 mM with 140 mM K^+ and 1 mM Mg-ATP in the intracellular (pipette) solution (2). Under these experimental conditions, K^+ currents are inward at potentials negative to the K^+ equilibrium potential (E_K, −23 mV; calculated by the Nernst equation) and exhibit strong rectification at potentials positive to E_K. To determine the effects of Arf6 inhibition on Kir2.1 currents over time, we included NAV-2729 (or DMSO) in the pipette to synchronize drug exposure with establishment of the whole-cell configuration. This design allowed us to analyze currents as a percentage of the initial (t_0) current amplitude, measured shortly after gaining electrical access to each cell. Importantly, t_0 Kir2.1 current densities were not significantly different between treatment groups (*SI Appendix*, Table S1). To accommodate the known loss of Kir2.1 activity over time following inhibition of PI4K and PIP5K, we performed our voltage ramp protocol every 2 min for 16 min, followed by addition of barium (Ba^{2+}), a selective Kir2 channel pore blocker at the concentration used (100 μM) (19). For each timepoint, a series of 20 voltage ramps was repeated, and the average maximum inward current at −140 mV was compared between treatments and timepoints.

As experimental treatments, we included 3 μM NAV-2729 (or equivalent volume of DMSO) in the patch pipette solution, with or without inclusion of the water-soluble PIP_2 analog, diC16-PIP_2 (10 μM), in the bath. With NAV-2729 in the pipette, Kir2.1 current density steadily decreased over time in cECs, dropping to 49 ± 4% of initial values within our 16-min recording window (Fig. 2 *B* and *C*). To confirm that the effect of NAV-2729 is specific to PIP_2 availability, we bypassed PIP5KI by bath-applying diC16-PIP_2, an external source of PIP_2 that enters cells and maintains Kir2.1 channel activity (20). The inclusion of diC16-PIP_2 in the bath preserved Kir2.1 currents in NAV-2729–treated cECs, maintaining current density at 90 ± 4% of its initial value. Consistent with our previous studies, Kir2.1 current density in cECs administered vehicle pipette solution remained stable (94 ± 1% of initial) throughout the recordings (Fig. 2*C* and *SI Appendix*, Fig. S1*A*) (19). These findings suggest that the effects of NAV-2729 on cEC Kir2.1 channel activity are specific to PIP_2 insufficiency.

To confirm the Arf6 specificity of NAV-2729 effects on PIP_2 and Kir2.1 currents in cECs, we employed our previously described tamoxifen-inducible, EC-specific Arf6-knockdown mouse (hereafter, $Arf6^{iECKD}$) which reduces EC Arf6 protein abundance by 30% (30). Using the conventional whole-cell patch-clamp configuration on brain cECs from these mice and their wild-type littermate controls, we sequentially performed two series of our voltage-ramp protocol—once under baseline conditions and once following addition of 100 μM Ba^{2+} to the bath. The Ba^{2+}-sensitive current was determined (Fig. 2*D*), and the difference in maximum inward current density between genotypes was calculated by normalization to whole-cell capacitance, which is proportional to cell surface area and was unchanged by genotype [10 ± 1 and 10 ± 2 pF in $Arf6^{fl/fl}$ (n = 7) and $Arf6^{iECKD}$ (n = 8) cells, respectively, from 3 mice each]. Kir2.1 current density was reduced by ~45% in cECs from $Arf6^{iECKD}$ mice compared to $Arf6^{fl/fl}$ littermates (Fig. 2 *D* and *E*). Bath application of diC16-PIP_2 restored currents in cECs from $Arf6^{iECKD}$ mice without affecting Kir2.1 currents in cECs from $Arf6^{fl/fl}$ control littermates (Fig. 2 *D* and *E*). In our 16-min voltage-ramp time course, NAV-2729 (3 μM) decreased Kir2.1 currents over time in $Arf6^{fl/fl}$ littermate controls (*SI Appendix*, Fig. S1 *B* and *C*). In contrast, it had no effect on Kir2.1 currents in cECs from $Arf6^{iECKD}$ mice, confirming that Arf6 is the primary molecular target of NAV-2729 at concentrations up to 3 μM, consistent with published reports (40). Together, these findings suggest that cEC Arf6 maintains basal PIP_2 production and sustains Kir2.1 channel activity.

Arf6 Inhibition Uncouples Capillary-To-Arteriole Electrical Signaling. cEC Kir2.1 channels are essential for sensing neuronal activity and propagating hyperpolarizing electrical signals from capillaries to feeding arterioles (2). Our observation that Arf6 inhibition decreased cEC Kir2.1 channel activity suggests that NAV-2729 could impair capillary-to-arteriole signaling and vasodilation. To test this, we evaluated NAV-2729 effects on capillary-to-arteriole electrical signaling and arteriole diameter in 3 to 4-mo-old wild-type mice by ex vivo pressure myography using our previously described capillary–parenchymal arteriole preparation, comprising a physiologically pressurized arteriole and intact capillaries (containing both cECs and pericytes) isolated from the middle cerebral artery (MCA) territory (Fig. 3*A*) (2). This preparation allows Kir2.1 channel-mediated electrical signal propagation between cECs to be monitored by locally elevating $[K^+]_o$ on capillary extremities (with osmolarity maintained by substituting Na^+) and measuring changes in the diameter of the upstream, attached arteriole segment (*SI Appendix*, Fig. S2*A*) (2). At baseline, all arterioles exhibited basal tone of 33 ± 3%, measured as constriction relative to maximum inner diameter, whether tone was induced by pressure (40 mm Hg) or using the thromboxane A2 analog and G_q-type G-protein-coupled receptor (G_qPCR) agonist, U-46619 (*SI Appendix*, Fig. S2*B*; see also *Methods*) (41). Kir2.1-mediated dilation was tested in all preparations by locally picospritzing artificial cerebrospinal fluid (aCSF) containing 10 mM K^+ onto the capillary bed by pressure ejection (Fig. 3 *A* and *B*). At baseline, all arterioles dilated following treatment of capillaries with 10 mM K^+; because this was true whether tone was induced by pressure or U-46619 (*SI Appendix*, Fig. S2*C*), results from both preparations were pooled. Subsequent treatment with NAV-2729 (1 μM, bath application) significantly reduced the dilatory response to capillary-applied K^+ in the attached, upstream arteriole, decreasing arteriole dilation to 28 ± 2% of maximum compared to 49 ± 7% with vehicle treatment (Fig. 3 *B* and *C* and *SI Appendix*, Table S2). These data suggest that Arf6 supports cEC-mediated capillary-to-arteriole electrical signaling.

Because quantification of capillary-to-arteriole electrical signaling is dependent on the degree of arteriole constriction, we tested whether NAV-2729 (0.1 to 1 μM) affected arteriole tone and

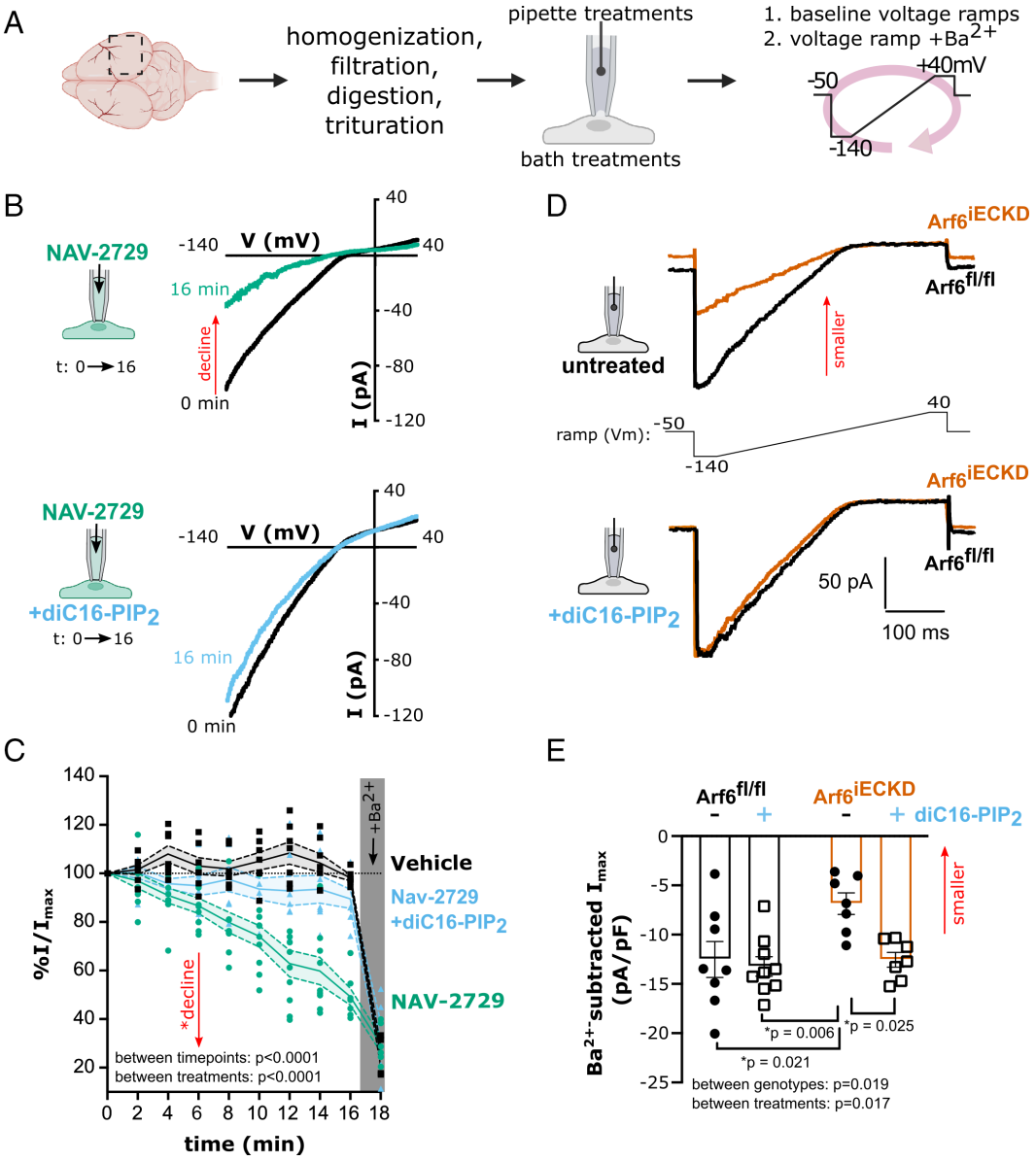

Fig. 2. Arf6 controls cEC Kir2.1 channel activity through PIP_2. (*A*) Schematic depicting the methodology for patch-clamp electrophysiology on freshly isolated brain cECs from the somatosensory cortex region. Experimental manipulations include mouse genotype and treatment via pipette and bath application. (*B*) Representative traces showing time-dependent changes in Kir2.1 currents (I, pA) in cECs from wild-type C57Bl/6J mice, recorded with NAV-2729 (3 μM; green) in the pipette, without (*Upper* panel) or with (*Lower* panel) diC16-PIP_2 (10 μM; blue) in the bath. (*C*) Summary data showing the percent change in maximal inward current for each time point and after final Ba^{2+} treatment, normalized to each cell's initial current multiplied by 100% and presented as means (solid line) ± SEM (dashed lines and filled area). Individual cells are shown as single datapoints [n = 6 to 7 cells per group from 3 male C57Bl/6J mice (3 to 4 mo old); mixed effects analysis with Geisser–Greenhouse correction: main effects of time, $F(2.39, 46.37) = 85.74$, $P < 0.0001$; treatment, $F(2, 21) = 20.64$, $P < 0.0001$; and interaction, $F(4.77, 46.37) = 10.07$, $P < 0.0001$]. Currents in NAV-2729–treated cells were significantly decreased relative to those in vehicle-treated cells for 4 to 16-min time points ($P < 0.05$) and were significantly decreased compared with PIP_2-supplemented cells for 8 to 16-min time points ($P < 0.05$). Ba^{2+} treatment significantly decreased currents relative to t_0 for all treatment conditions (Tukey's multiple comparisons test). (*D*) Representative Ba^{2+}-subtracted Kir2.1 currents in cECs from $Arf6^{fl/fl}$ (black) and $Arf6^{iECKD}$ (orange) mice, recorded in the conventional whole-cell configuration, for untreated cells (*Top*) and cells treated with bath-applied diC16-PIP_2 (*Bottom*). (*E*) Summary data showing effects of bath-applied diC-16-PIP_2 on Kir2.1 currents in $Arf6^{fl/fl}$ and $Arf6^{iECKD}$ mice. Data are presented as means ± SEM [n = 7 to 9 cells from 3 mice per treatment condition; two-way ANOVA with Tukey's multiple comparison post hoc test: interaction main effect, $F(1, 27) = 3.883$, $P = 0.059$; genotype main effect, $F(1, 27) = 6.277$, $P = 0.019$; treatment main effect, $F(1, 27) = 6.439$, $P = 0.017$].

confirmed that it did not (Fig. 3*D* and *SI Appendix*, Table S3). These findings suggest that NAV-2729 in this concentration range does not impair SMC constriction.

EC Arf6 Inhibition Impairs Kir2.1-Mediated Functional Hyperemia by Reducing the Availability Of PIP_2. To test whether Arf6-driven PIP_2 production supports Kir2.1-mediated functional hyperemia, we measured CBF changes in response to whisker stimulation in anesthetized C57Bl/6J mice equipped with an acute cranial window (Fig. 4*A*). We defined functional hyperemia as the percent increase in CBF relative to the prestimulation baseline and controlled for intersubject variability by comparing functional hyperemic responses within the same animal before and after a given treatment. Cortical application of the Arf6 inhibitor, NAV-2729 (3 μM) significantly decreased functional hyperemic responses from 20 ± 1% before treatment to 9 ± 1% after treatment (Fig. 4*B*). In contrast, functional hyperemic responses to whisker stimulation were elevated after application of vehicle (25 ± 2%) compared with pretreatment values (22 ± 2%) (Fig. 4*C* and *SI Appendix*, Fig. S3*A*). This modest increase in functional

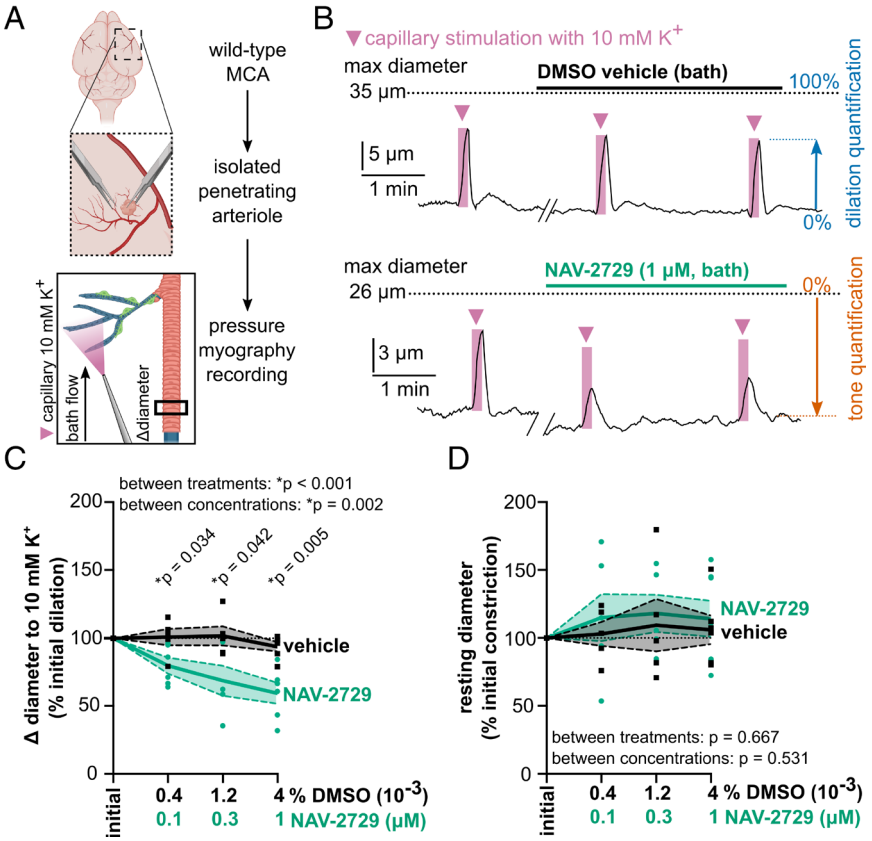

Fig. 3. Arf6 inhibition with NAV-2729 decreases arteriole dilation in response to application of 10 mM K^+ to capillary extremities. (*A*) Schematic of the preparation for pressure myography measurement of arteriole tone (prestimulation) and dilation to capillary-applied 10 mM K^+. (*B*) Representative traces showing arteriole dilation in response to localized picospritzing of capillary extremities with 10 mM K^+ for 10 s under initial conditions and after vehicle (*Upper* trace) or NAV-2729 (1 µM; *Lower* trace) application. (*C*) Summary data showing percent change in arteriole dilation in response to focal capillary application of 10 mM K^+, normalized to initial response multiplied by 100% [mixed effects analysis with Geisser–Greenhouse correction: main effects of treatment, F(1,13) = 21.95, P = < 0.001; concentration, F(2.17, 19.53) = 8.881, P = 0.002; and interaction, F(2.17, 19.53) = 5.924, P = 0.009; P < 0.05 for NAV-2729 vs. equivolume DMSO, Tukey's multiple comparisons test (all treatment concentrations)]. (*D*) Summary data showing percent change in arteriole tone between vehicle and NAV-2729 treatment, normalized to initial tone multiplied by 100% [mixed effects analysis with Geisser–Greenhouse correction: main effects of treatment, F(1,14) = 1.193, P = 0.667; concentration, F(2.05, 19.16) = 0.663, P = 0.531; and interaction, F(2.05, 19.16) = 0.169, P = 0.851; no post hoc test]. All data are presented as means ± SEM [N = 5 to 8 male C57Bl/6J mice (3 to 4 mo old)] and are displayed as individual data points.

hyperemic responses was not observed using a 10-fold lower concentration of DMSO vehicle (*SI Appendix*, Fig. S3 *B* and *C*), so is likely attributable to elevated DMSO.

To determine whether NAV-2729-induced reductions in hyperemic responses are attributable to impaired PIP_2 availability, we supplemented diC16-PIP_2 via intravenous (i.v.) administration, a maneuver that directly delivers PIP_2 to ECs and bypasses the need for endogenous Arf6-mediated PIP_2 production (20). Concurrent administration of diC16-PIP_2 rescued NAV-2729 (3 µM)-induced functional hyperemia deficits, yielding increases (16 ± 1%) comparable to those observed prior to treatment (18 ± 1%) (Fig. 4 *B* and *C*). Similar decreases in functional hyperemic responses were obtained with a lower concentration of NAV-2729 (0.3 µM), reductions that were likewise prevented by i.v. diC16-PIP_2 (*SI Appendix*, Fig. S3 *B* and *C*).

To test whether the effects of NAV-2729 are localized to the vascular endothelium, we next compared Kir2.1-dependent functional hyperemic responses between *Arf6*^{iECKD} mice and *Arf6*$^{fl/fl}$ littermate controls. Baseline functional hyperemic responses were significantly lower in *Arf6*^{iECKD} mice (16 ± 1%) than in *Arf6*$^{fl/fl}$ mice (20 ± 2%) (Fig. 4 *D* and *E*). We then quantified the Kir2.1-dependent component of the response within each genotype by subsequently applying Ba^{2+} (100 µM) to the superfusate. Ba^{2+} reduced functional hyperemia to a greater extent in *Arf6*$^{fl/fl}$ mice (47 ± 4%) than in *Arf6*^{iECKD} mice (26 ± 5%), indicating a diminished Kir2.1 contribution to functional hyperemia in *Arf6*^{iECKD} mice (Fig. 4*F*).

In an independent cohort, we confirmed the functional hyperemia deficit in *Arf6*^{iECKD} mice and directly tested rescue by i.v. PIP_2 supplementation. diC16-PIP_2 (i.v.) increased functional hyperemic responses in *Arf6*^{iECKD} mice from 12 ± 1% (pretreatment) to 17 ± 1% (posttreatment). Following diC16-PIP_2 administration, functional hyperemic responses in *Arf6*^{iECKD} mice were statistically indistinguishable from those in *Arf6*$^{fl/fl}$ littermates receiving the same treatment (Fig. 4 *G* and *H*). Together, these data demonstrate that endothelial Arf6 is required to sustain PIP_2 production, maintain Kir2.1 channel function, and support normal functional hyperemia.

Discussion

The brain operates on the brink of energy insufficiency, placing considerable pressure on autoregulatory mechanisms responsible for maintaining basal blood flow and sensitizing neuronal function to metabolic challenges such as diabetic hypoglycemia and insufficient CBF (42, 43). Layered on top of these constitutive energy requirements are dynamic changes in brain energy demand driven by spatial and temporal variations in neuronal activity (44). In the somatosensory cortex, these latter changes are met by neurovascular coupling mechanisms that elicit functional hyperemia (45).

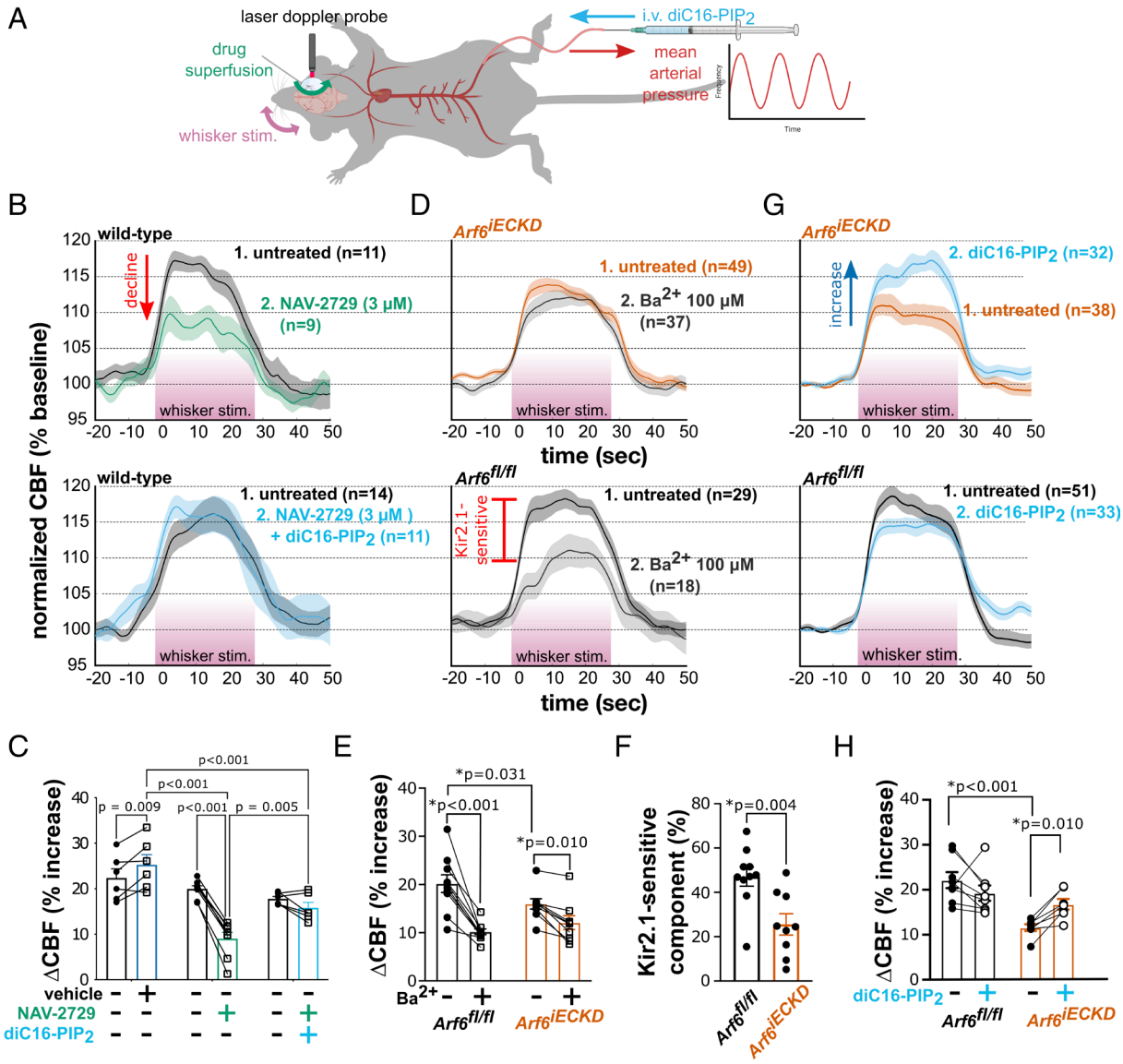

Fig. 4. Arf6 loss impairs Kir2.1-mediated functional hyperemic responses to whisker stimulation and PIP_2. (*A*) Experimental schematic of laser Doppler flowmetry over a somatosensory cortex cranial window. Whisker stimulation (pink) was performed in technical replicates after each treatment. (*B*) Summary CBF traces for sequential recordings obtained at baseline and after cortical superfusion with vehicle, 3 μM NAV-2729, or 3 μM NAV-2729 + 0.5 mg/kg diC16-PIP_2, normalized to prestimulation baseline. Timing of whisker simulation denoted by pink underline. Paired treatments are superimposed. Whisker stimulation technical replicates (n) for all 4 to 7 animals (N) are shown as means ± SEM. (*C*) Summary data showing paired CBF responses to whisker stimulation under treatment and control conditions. For all panels, each data point represents the average change in CBF following whisker stimulation per treatment per individual animal [N = 6 to 8 mice; repeated-measures, two-way ANOVA: main effects of drug treatment, F(2,17) = 12.74, $P = 0.0004$; timepoint, F(1,17) = 36.93, $P < 0.0001$; interaction, F(2,17) = 59.09, $P < 0.0001$; and subject, F(17,17) = 8.236, $P < 0.0001$; Tukey's multiple comparisons test, $P < 0.05$, displayed]. (*D*) Summary traces showing CBF changes in response to whisker stimulation, before and after Ba^{2+} superfusion (20 min), in $Arf6^{fl/fl}$ and $Arf6^{iECKD}$ mice. Whisker stimulation technical replicates (n) for all 9 to 10 animals (N) are shown as means ± SEM. (*E*) Summary data showing paired CBF responses to whisker stimulation, with and without Ba^{2+} treatment, in $Arf6^{fl/fl}$ (N = 10) and $Arf6^{iECKD}$ (N = 9) mice [repeated-measures, two-way ANOVA: main effects of genotype, F(1,17) = 0.504, $P = 0.487$; treatment, F(1, 17) = 56.33, $P < 0.0001$; and interaction, F(1, 17) = 10.91, $P = 0.004$; uncorrected Fisher's LSD post hoc test, $P < 0.05$, displayed]. (*F*) Summary data showing the Ba^{2+}-sensitive component of the total functional hyperemic response multiplied by 100%; same subjects as in *D* and *E* [unpaired *t* test; t(17) = 3.341]. (*G*) Summary traces showing CBF changes in response to whisker stimulation, with and without diC16-PIP_2 administration (0.5 mg/kg, i.v.), in $Arf6^{fl/fl}$ and $Arf6^{iECKD}$ mice. Whisker stimulation technical replicates (n) for all 7 to 8 animals (N) are shown as means ± SEM. (*H*) Summary data showing paired CBF responses to whisker stimulation (untreated, plus diC16-PIP_2) in $Arf6^{fl/fl}$ (N = 8) and $Arf6^{iECKD}$ (N = 7) mice. Data are presented as means ± SEM [repeated-measures, two-way ANOVA: main effects of genotype, F(1,13) = 14.47, $P = 0.0022$; treatment, F(1, 13) = 0.9563, $P = 0.346$; and interaction main effect, F(1, 13) = 11.72, $P = 0.005$; uncorrected Fisher's LSD post hoc test, $P < 0.05$, displayed].

Functional hyperemia deficits coincide with cEC PIP_2 insufficiency in cSVD models (7, 20, 21). Yet the mechanisms of PIP_2 synthesis remain unexplored in cECs and incompletely understood generally. Using Kir2.1 channel activity as an index for PIP_2 availability, we show that Arf6 is required to maintain physiological levels of PIP_2 in cECs. Our data also provide evidence for a direct and causal relationship between EC PIP_2 homeostasis and CBF regulation, as impairing PIP_2 metabolism through Arf6 was sufficient to drive functional hyperemia deficits. Collectively, these findings position EC Arf6 as an "Achilles heel" in PIP_2 synthesis and a new target for treating CBF deficits observed in cSVDs.

The striking effect of Arf6 inhibition on Kir2.1 channel activity suggests that Arf6 controls the rate of PIP5KI activity. Arf6 inhibition decreased cEC Kir2.1 currents by ~50%, and Arf6 knockdown decreased Kir2.1 current density by ~45% (Fig. 2). By comparison, our previous electrophysiological studies showed that precluding PIP_2 synthesis through PI4K inhibition, PIP5K inhibition, or removal of ATP from the intracellular (pipette) solution causes a

~30 to 40% decline in cEC Kir2.1 currents (19). In other words, inhibiting Arf6 impaired Kir2.1 channel activity to a similar degree as directly inhibiting the enzymes responsible for PIP_2 production. The strong effect of Arf6 on apparent PIP_2 availability was initially surprising considering that PIP5KI, the primary target of Arf6 in the PIP_2 synthesis pathway, is not considered a rate-limiting enzyme (15). Indeed, elegant studies by the Hille group using an exogenous expression system showed that PIP_2-dependent K_V7 channel activity recovers rapidly ($t_{1/2}$ max current within ~10 s) following PIP_2 conversion to PIP by PIP5KI (46), but takes ~12 times longer ($t_{1/2}$ max current > 2 min) following PLC-mediated PIP_2 depletion. This prolonged recovery time reflects the required engagement of both PI4K and PIP5KI to replenish PIP_2 and has defined PI4K as the rate-limiting step for PIP_2 synthesis. While PI4K is a rate-defining step, our data suggest that we should not place too fine a point on this distinction. Indeed, colocalized PI4K and PIP5K synergize PIP_2 synthesis (15), underscoring the concept of multiple rate-controlling steps in metabolic pathways.

PIP5KI activity robustly adapts to maintain PIP_2 steady-state levels. Modeling suggests that PIP5KI activity increases up to 500-fold during prolonged PLC-mediated conversion of PIP_2 to inositol triphosphate and diacylglycerol (15, 47). While the mechanisms underlying this massive dynamic range remain incompletely characterized, our data support a key role for Arf6. Notably, Arf6 can increase PIP5KI activity ~10-fold—and up to ~40 to 60-fold when combined with phosphatidic acid (a byproduct of diacylglycerol)—in reconstituted cytosol systems (26, 48). Additionally, the Arf6 GTP-cycle regulates PIP5KI localization at the plasma membrane, where increased substrate availability, PIP_2-mediated positive feedback, and dimerization potentiate PIP5KI activity (26, 27, 47, 49, 50). Finally, Arf6 activation of PIP5KI serves as an intrinsic negative feedback mechanism against PIP_2 depletion by PLC (used in the classic Hille kinetic assays) (15, 51, 52). Through these varied mechanisms, Arf6 insufficiency can disrupt PIP5KI activity and/or localization to block the final step in PIP_2 synthesis. Besides bulk pool sizes, spatiotemporally coupled fluctuations in PIP_2 abundance—coined "oscillations"—have recently been linked to cytoskeleton dynamics (53). Although these oscillations are driven by PI4K-type kinase, whether Arf6 impacts PIP_2 pool sizes or oscillations remains an important outstanding question.

Our data also expand on existing models of dynamic PIP_2 turnover in cECs. Indeed, the classical phenomenon of ion channel activity "run down" due to a mismatch between ongoing PIP_2 depletion and stunted PIP_2 synthesis in excised membrane patch recordings has helped to identify many PIP_2-modulated ion channels (16, 54). Such continuous PIP_2 consumption also occurs in native cECs, as illustrated by the observation that impairing PIP_2 synthesis decreases cEC Kir2.1 channel activity over time (19). Notably, none of our electrophysiological recordings involved protocols that drove PIP_2 depletion; thus, in addition to supporting existing evidence for basal PIP_2 consumption, our findings introduce Arf6 as a basal regulator of PIP_2 homeostasis in cECs (Figs. 1–3).

cECs appear uniquely susceptible to PIP_2 insufficiency. Loss of Kir2.1 channel activity in cSVD models is specific to brain cECs; arterial/arteriolar ECs do not show corresponding deficits (20). Proteomic and immunocytochemical analyses show that Arf6 protein abundance progressively decreases with age in cECs while remaining unchanged in isolated capillaries, which also contain pericytes, astrocyte endfeet, and synaptic terminals (30). Readouts from our complementary preparations spanning isolated cECs to intact cell-specific knockdown mice strengthen our conclusion that EC Arf6 permits capillaries to conduct hyperpolarizing, vasodilatory signals by sustaining PIP_2 levels. Our data do not preclude other roles for Arf6 in additional cells of the neurovascular unit (55, 56). This possibility is highlighted by our finding that diC16-PIP_2 restored functional hyperemia to wild-type levels in *Arf6*^{iECKD} mice, yet failed to rescue functional hyperemia to vehicle-treated levels when coadministered with cortical NAV-2729. Emerging evidence suggests that the kinetic and steady state properties of phosphoinositide metabolism vary by cell type, with faster synthesis and larger PIP precursor pool sizes in excitable primary neurons compared with nonexcitable primary astrocytes and cultured cells (e.g., tsA201 cells) (15, 57). The evidence for cell-type specific disease and age-driven changes in PIP_2 synthesizing machinery and the activity of PIP_2-dependent ion channels underscores the importance of defining the kinetics of phosphoinositide synthesis in vascular cells (20, 30).

From a therapeutic standpoint, most studies on Arf6 have focused on decreasing aberrantly high Arf6 activity in models of cancer, diabetic retinopathy, sepsis, and neurodegeneration (33, 40, 58–62). However, the emerging roles for Arf6 in vasodilatory responses make it clear that any therapy aimed at normalizing Arf6 in disease should do just that—normalize Arf6—no more and no less. Our inducible knockdown model shows that even modest (~30%) reductions in Arf6 mRNA in capillaries and protein abundance in isolated cECs are sufficient to significantly impair functional hyperemic responses (30). Interesting in this context, Arf6 protein abundance is significantly decreased (~18%) in capillaries of CADASIL patients compared with aged-matched control subjects (31). Future work will aim to confirm the pathophysiological relevance of this latter observation and determine whether restoring Arf6 expression and function ameliorates CBF deficits in cSVDs.

Our findings provide evidence that Arf6 in brain ECs sustains PIP_2 levels sufficient for Kir2.1-mediated electrical signaling. However, we did not investigate other pathways through which Arf6 might control EC function, including EC-derived signaling molecules (e.g., nitric oxide and prostanoids), additional PIP_2-regulated ion channels (e.g., TRPV4, TRPA1, and Piezo1), or PIP_2-consuming intracellular signaling cascades (e.g., G_qPCRs and PI3K/AKT signaling) (15, 16, 63–65). Hinting at roles for these latter pathways, a recent study by Islam et. al. showed that EC-mediated dilatory responses to insulin are lost in skeletal and adipose tissue vessels from *Arf6*^{iECKD} mice, but G_qPCR-mediated dilation to acetylcholine is retained (35). These findings suggest that insulin activation couples with Arf6 within the receptor tyrosine kinase and PI3K/AKT signaling cascade. Indeed, others have shown that activation of the receptor tyrosine kinase, ROR2, increases PIP5KI and PIP_2 at the plasma membrane (66). Thus, how Arf6 undergirds different EC signaling pathways through maintenance of PIP_2 availability warrants further investigation.

Because PIP_2 is required for the function of Kir2.1 channels, which underlie electrical signaling-based functional hyperemia, cEC PIP_2 availability is a major determinant of dynamic fluctuations in CBF. Here, we found that EC Arf6 controls PIP_2 availability and that its pharmacological inhibition or EC-specific genetic knockdown is sufficient to disrupt EC Kir2.1 channel activity and functional hyperemia. Our findings suggest that endothelial cell PIP_2 unavailability precipitates functional hyperemia deficits and that Arf6 may thus represent a disease-altering therapeutic target. Accordingly, if PIP_2 is the "coin of the realm" for ion channel activity, then Arf6 might be the "mint" (67).

Materials and Methods

Chemicals. diC16-PIP_2 [PtdIns-(4, 5)-P2 (1,2-dipalmitoyl), sodium salt] and U-46619 were obtained from Cayman Chemical Company. All other chemicals, including NAV-2729, were obtained from Millipore-Sigma, unless otherwise

stated. NAV-2729 partitions into lipid membranes when added to aqueous solutions and inhibits Arf6-GEF activity with low micromolar potency (1.0 to 3.4 μM), but also inhibits Arf GEFs and GAPs with intermediate potency (2.7 to >50 μM) and binds promiscuously to pleckstrin homology domains with lower potency (250 μM). Our studies use ≤3.0 μM NAV-2729 complemented with rescue experiments and control experiments in Arf6 knockdown cells.

Animal Models. All experiments reported in this study were performed at the University of Vermont in accordance with institutional and ARRIVE guidelines and with the approval of the Institutional Animal Care and Use Committee of the University of Vermont. Mice were group-housed on a 12-h light/dark cycle with ad libitum delivery of food and water. Adult (3 to 4-mo-old) male C57/Bl6J mice were acquired from The Jackson Laboratory (Bar Harbor, ME). Dual-reporter mice expressing green fluorescent protein (GFP) in ECs and red fluorescent protein in SMCs and pericytes, hereafter referred to as EC/SMC reporter mice, were created by crossing *Cdh5*-GCaMP8 and *Acta2*-RCaMP mice (both from Jackson Laboratory; CHROMus collaboration) and used to validate capillary purity in independent experiments. EC-specific *Arf6* knockdown (*Arf6*^{iECKD}) mice were generated by crossing B6.CgArf6tm.11GDP/J mice (*Arf6*$^{fl/fl}$; Jackson 028669) with Tg(*Cdh5*-Cre^{ERT2})1Rha mice (a kind gift from Ralf H. Adams), as described previously (30). Arf6 deletion was induced by treating *Arf6*^{iECKD} mice with 2 mg tamoxifen/mouse/d for 5 d; *Arf6*$^{fl/fl}$ littermates were treated identically. Mice were used at 3 to 4 mo of age (minimum 1 mo of tamoxifen washout). For C57/Bl6J mouse experiments, only male mice were used. These experiments were complemented by experiments in *Arf6*$^{fl/fl}$ and *Arf6*^{iECKD} mice that included both males and females. For experiments with *Arf6*$^{fl/fl}$ and *Arf6*^{iECKD} mice, experimenters were blinded to mouse genotype only. There were no differences in bodyweight between *Arf6*$^{fl/fl}$ and *Arf6*^{iECKD} mice (*SI Appendix*, Fig. S4*A*). Baseline functional hyperemic responses within each genotype did not differ according to biological sex (*SI Appendix*, Fig. S4*B*); thus, males and females were pooled throughout. Mice were randomized to treatment groups based on birth order, and design was counterbalanced across treatment conditions.

PIP5KI Activity Assay. Brain capillary preparations were obtained by density gradient centrifugation using previously reported protocols as described in *SI Appendix, Supplemental Methods* (39). Freshly isolated brain capillaries were resuspended in HEPES-buffered (pH 7.4) Dulbecco's Modified Eagle Medium (DMEM) base medium (Agilent, Santa Clara, CA) containing 4 mM glucose, 1 mM pyruvate, and 2 mM L-alanyl-L-glutamine. After adding 3 μM NAV-2729 or vehicle (0.01% DMSO), vessel suspensions were incubated for 20 min at 37 °C with constant mixing. At the end of the incubation, vessels were diluted 1:1 in ice-cold base medium, pelleted by centrifuging at 2,000×*g* for 10 min at 4 °C, and flash frozen. Capillaries were homogenized in ice-cold RIPA buffer (9806S; Cell Signaling Technology, Danvers, MA) supplemented with protease and phosphatase inhibitors. Insoluble fractions were removed by centrifugation at 14,000×*g* for 10 min at 4 °C. Equal amounts of capillary protein lysate (estimated by bicinchoninic acid assay) were tested for PIP5KI activity according to instructions provided by the kit manufacturer (K-5700; Echelon Biosciences, Inc., Salt Lake City, UT). In this assay, ATP is limiting and PIP5KI activity is driven by supplementing capillary lysates with excess PIP substrate and cofactors. At the end of the assay, enzymatic activity is quenched, and PIP5KI activity in the sample is calculated as the inverse of the remaining (ATP), determined by reference to a standard curve, and averaged across technical replicates. To control for batch-to-batch variation, we normalized residual (ATP) to the average vehicle signal per assay. Protein input and incubation time were determined in independent pilot assays (not shown).

Electrophysiology. Freshly isolated brain cECs were patched in the conventional whole-cell configuration as described previously; solution compositions and additional details are provided in *SI Appendix, Supplemental Methods* (2). For PIP_2 rescue experiments, 10 μM diC16-PIP_2 was included in the bath solution, and cells were incubated for 20 min prior to patch clamping. The pipette solution contained either 3 μM NAV-2729 or vehicle (0.01% DMSO). After gaining electrical access to a single cEC, we performed twenty, 400-ms voltage ramps every 2 min for a total of 16 min. At the end of each 16-minute recording, 100 μM Ba^{2+} was added to the bath to inhibit Kir2 channel activity. Whole-cell currents were normalized to whole-cell capacitance, determined through the cancellation circuitry in the voltage-clamp amplifier.

Myography. Parenchymal cerebral arterioles with attached capillary beds were dissected from the middle cerebral artery as previously described and outlined in the *SI Appendix, Supplemental Methods* (2). Tone was induced by applying physiological pressure (40 mmHg). A micropipette filled with aCSF containing 10 mM KCl (substituted for NaCl) was attached to a Pneumatic PicoPump picospritzer (World Precision Instruments, Sarasota, FL) positioned in front of the capillary bed, oriented in the direction of the bath flow. In this configuration, a 10 mM KCl pipette solution pressure-ejected at 10 psi for 10 s targets the capillary bed only (*SI Appendix*, Fig. S2*A*), so changes in arteriole diameter are attributable to capillary-to-arteriole communication (2). In a subset of preparations, pressure-induced tone was increased by treating with the thromboxane A2 analog, U-46619 (200 nM), which constricts vessels to the same degree as pressure (*SI Appendix*, Fig. S2*B*). As both vessels with myogenic tone and U-46619-induced preconstriction exhibited the same degree of arteriole dilation to capillary 10 mM K^+ (*SI Appendix*, Fig. S2*C*), vessels with myogenic tone and those treated with U-46619 were pooled for subsequent analysis. Changes in lumen diameter are presented as the change in internal (lumen) diameter over the 10 s of treatment, normalized to the difference between maximal internal diameter in 0 mM Ca^{2+} aCSF (applied at the end of each protocol) and the prestimulated diameter, calculated as (change in diameter)/(maximal diameter – prestimulated diameter) x 100%. Tone was calculated as (prestimulated diameter)/(maximal diameter) x 100%.

In Vivo Laser-Doppler Flowmetry. Acute cranial windows were generated as previously described (2) and detailed in *SI Appendix, Supplemental Methods*. Blood pressure was continuously monitored at 200 Hz via a femoral artery cannula and was unchanged between genotypes (*SI Appendix*, Fig. S4*C*). Nonfasted blood glucose in blood samples collected at the end of experiments was analyzed using an epoc Reader (Siemens Healthineers, Ottawa, Canada) and BGEM test cards (Siemens Healthcare Diagnostics, Dublin, Ireland). No differences were detected between *Arf6*$^{fl/fl}$ and *Arf6*^{iECKD} mice (*SI Appendix*, Fig. S4*D*) (35). Functional hyperemia was induced by manually brushing the contralateral vibrissae, and responses were aligned to the event onset (defined in *SI Appendix, Supplemental Materials*) and compiled for summary data. The manual stimulation paradigm precludes defining response kinetics, so the peak average response during stimulation was reported. In controls testing inherent experimenter variability in this manual stimulation paradigm, the same stimulation of the ipsilateral vibrissae induced only a ~5% CBF change (*SI Appendix*, Fig. S5). If whisker stimulation failed to induce an increase in CBF greater than 5% of prestimulation levels across the exposed cortical surface, the animal was excluded from further experiments.

For acute treatments, NAV-2729 or DMSO vehicle was added to the aCSF superfusate for 20 min after performing baseline recordings. Ba^{2+}-sensitive responses to whisker stimulation were obtained by treating for 20 min with Ba^{2+} (100 μM), added to the cortical superfusate. All whisker stimulation responses, recorded in arbitrary units, were analyzed using LabChart software (ADInstruments, Dunedin, New Zealand) and are presented as the percent change in CBF from prestimulation values, averaged over three whisker stimulation trials per treatment condition. The Ba^{2+}-sensitive functional hyperemic response was determined by subtracting functional hyperemic responses under Ba^{2+} treatment from untreated baseline, then multiplying the result by 100%.

Statistical Analysis. Excel was used for data preprocessing. GraphPad Prism version 10 was used for statistical analyses. Biological outliers were excluded using Grubb's Test. Data distribution was tested with the Shapiro–Wilk's normality test. Statistical tests (all two tailed) are indicated in figure legends. *t* test results are reported as critical t-value and degrees of freedom (in parentheses). Main effects from ANOVA tests are reported as F-value, degrees of freedom (numerator, denominator), and p-value. Associated post hoc tests are reported as multiplicity-adjusted *P*-values. Data are presented as means ± SEM. Differences between means with *P*-values < 0.05 were considered statistically significant.

Data, Materials, and Software Availability. All study data are included in the article and/or supporting information.

ACKNOWLEDGMENTS. We thank O. Harraz, L. Schröger, D. Paquet, and J. Gonzalez-Gallego for designing and performing initial pilot experiments; G. Herrera for making the initial MATLAB code for plotting CBF responses; G. Hennig for helpful discussions on data preprocessing; O. Nadeau for editing the manuscript; and S. Tighe, N. Cashen, T. Wellman, and T. Classen for technical assistance. Research reported in this publication was supported by the Leducq Foundation

Transatlantic Network of Excellence (International Network of Excellence on Brain Endothelium: A Nexus for Cerebral Small Vessel Disease 22CVD01 BRENDA, to M.D. and M.T.N.), the Totman Medical Research Trust (M.T.N.), and grants from the National Institute of Neurological Disorders and Stroke (R01-NS-110656 and RF1-NS-128963 to M.T.N; R01-NS140868 to M.K; R01-NS-119971 to Nicholas Tsoukias and M.T.N subcontracted), the National Heart Lung and Blood Institute (R35-HL-140027 to M.T.N.), The Spanish Ministry of Science and Innovation (PID2023-147925OA-I00 to M.S.), the American Heart Association (24POST1188081 to S.H.d.l.C.), the Deutsche Forschungsgemeinschaft (DFG; German Research Foundation) as part of the Munich Cluster for Systems Neurology (EXC 2145 SyNergy–ID 390857198), CRC 1744 (ID 548585053), DI 722/13-1, and DI 722/21-1; the flagship P4-medicine project DigiMed Bayern; ERA-NET Neuron (MatriSVDs, to M.D.); and the Vascular Dementia Research Foundation. Technical support for qPCR was provided by the Advanced Genome Technologies Core of the University of Vermont and the Larner College of Medicine: Vermont Integrative Genomics Resource Facility (RRID# SCR_021775). NIH funds solely supported research in Vermont. No NIH funds supported foreign collaborators at foreign institutions. Figures were created in BioRender. Noterman, M. (2026): https://BioRender.com/nplbrcw.

Author affiliations: [a]Department of Pharmacology, University of Vermont, Burlington, VT 05405; [b]Department of Physiology, Universidad Complutense de Madrid, Madrid 28040, Spain; [c]Department of Biology, Ecology and Earth Sciences, University of Calabria, Calabria 87036, Italy; [d]Department of Translational Stroke and Dementia Research, Institute for Stroke and Dementia Research, University Hospital, Ludwig-Maximilians-Universität, Munich 81377, Germany; [e]Munich Cluster for Systems Neurology, Munich 81377, Germany; [f]German Centre for Neurodegenerative Diseases, Munich 81377, Germany; [g]German Centre for Cardiovascular Research, Munich 81377, Germany; and [h]Division of Cardiovascular Sciences, University of Manchester, Manchester M13 9NT, United Kingdom

Author contributions: M.F.N.-S., M.S., and M.T.N. designed research; M.F.N.-S., M.S., S.H.d.l.C., M.Y., M.M., M.K., and E.M. performed research; N.B., K.T.-V., and M.D. contributed new reagents/analytic tools; M.F.N.-S., M.S., S.H.d.l.C., M.Y., M.M., and E.M. analyzed data; and M.F.N.-S., D.H.-E., and M.T.N. wrote the paper.

1. B. R. Chen, M. G. Kozberg, M. B. Bouchard, M. A. Shaik, E. M. C. Hillman, A critical role for the vascular endothelium in functional neurovascular coupling in the brain. *J. Am. Heart Assoc.* **3**, e000787 (2014).
2. T. A. Longden *et al.*, Capillary K+-sensing initiates retrograde hyperpolarization to increase local cerebral blood flow. *Nature Neurosci.* **20**, 717–726 (2017).
3. R. L. Rungta, E. Chaigneau, B.-F. Osmanski, S. Charpak, Vascular compartmentalization of functional hyperemia from the synapse to the pia. *Neuron* **99**, 362–375.e364 (2018).
4. É. Martineau, A. Malescot, N. Elmkinssi, R. L. Rungta, Distal activity patterns shape the spatial specificity of neurovascular coupling. *Nature Neurosci.* **27**, 2101–2114 (2024).
5. M. Koide *et al.*, Differential restoration of functional hyperemia by antihypertensive drug classes in hypertension-related cerebral small vessel disease. *J. Clin. Investig.* **131**, e149029 (2021).
6. H. R. Ferris *et al.*, Epidermal growth factor receptors in vascular endothelial cells contribute to functional hyperemia in the brain. *Int. J. Mol. Sci.* **24**, 16284 (2023).
7. A. Mughal, O. F. Harraz, A. L. Gonzales, D. Hill-Eubanks, M. T. Nelson, PIP(2) improves cerebral blood flow in a mouse model of Alzheimer's disease. *Function (Oxf)* **2**, zqab010 (2021).
8. A. Moshkforoush *et al.*, The capillary Kir channel as sensor and amplifier of neuronal signals: Modeling insights on K+-mediated neurovascular communication. *Proc. Natl. Acad. Sci.* **117**, 16626–16637 (2020).
9. G. G. Somjen, Extracellular potassium in the mammalian central nervous system. *Annu. Rev. Physiol.* **41**, 159–177 (1979).
10. Y. Yamamoto, M. F. Klemm, F. R. Edwards, H. Suzuki, Intercellular electrical communication among smooth muscle and endothelial cells in guinea-pig mesenteric arterioles. *J. Physiol.* **535**, 181–195 (2001).
11. H. J. Knot, M. T. Nelson, Regulation of arterial diameter and wall [Ca2+] in cerebral arteries of rat by membrane potential and intravascular pressure. *J. Physiol.* **508**, 199–209 (1998).
12. G. G. Emerson, S. S. Segal, Electrical coupling between endothelial cells and smooth muscle cells in hamster feed arteries. *Circ. Res.* **87**, 474–479 (2000).
13. C.-L. Huang, S. Feng, D. W. Hilgemann, Direct activation of inward rectifier potassium channels by PIP2 and its stabilization by Gβγ. *Nature* **391**, 803–806 (1998).
14. S. B. Hansen, X. Tao, R. MacKinnon, Structural basis of PIP2 activation of the classical inward rectifier K+ channel Kir2.2. *Nature* **477**, 495–498 (2011).
15. J. B. Jensen *et al.*, Biophysical physiology of phosphoinositide rapid dynamics and regulation in living cells. *J. General Physiol.* **154**, e202113074 (2022).
16. O. F. Harraz, D. Hill-Eubanks, M. T. Nelson, PIP2: A critical regulator of vascular ion channels hiding in plain sight. *Proc. Natl. Acad. Sci.* **117**, 20378–20389 (2020).
17. D. W. Hilgemann, Local PIP 2 signals: When, where, and how? *Pflug. Arch. Eur. J. Physiol.* **455**, 55–67 (2007).
18. C. Nasuhoglu *et al.*, Nonradioactive analysis of phosphatidylinositides and other anionic phospholipids by anion-exchange high-performance liquid chromatography with suppressed conductivity detection. *Anal. Biochem.* **301**, 243–254 (2002).
19. O. F. Harraz, T. A. Longden, F. Dabertrand, D. Hill-Eubanks, M. T. Nelson, Endothelial GqPCR activity controls capillary electrical signaling and brain blood flow through PIP2 depletion. *Proc. Natl. Acad. Sci.* **115**, E3569–E3577 (2018).
20. F. Dabertrand *et al.*, PIP2 corrects cerebral blood flow deficits in small vessel disease by rescuing capillary Kir2. 1 activity. *Proc. Natl. Acad. Sci.* **118**, e2025998118 (2021).
21. P. Thakore *et al.*, PI3K block restores age-dependent neurovascular coupling defects associated with cerebral small vessel disease. *Proc. Natl. Acad. Sci.* **120**, e2306479120 (2023).
22. H. S. Markus, A. Joutel, The pathogenesis of cerebral small vessel disease and vascular cognitive impairment. *Physiol. Rev.* **105**, 1075–1171 (2025).
23. R. A. Kahn, A. G. Gilman, The protein cofactor necessary for ADP-ribosylation of Gs by cholera toxin is itself a GTP binding protein. *J. Biol. Chem.* **261**, 7906–7911 (1986).
24. S. E. Langille *et al.*, ADP-ribosylation factor 6 as a target of guanine nucleotide exchange factor GRP1. *J. Biol. Chem.* **274**, 27099–27104 (1999).
25. J. Gaschet, V. W. Hsu, Distribution of ARF6 between membrane and cytosol is regulated by its GTPase cycle. *J. Biol. Chem.* **274**, 20040–20045 (1999).
26. A. Honda *et al.*, Phosphatidylinositol 4-phosphate 5-kinase α is a downstream effector of the small G protein ARF6 in membrane ruffle formation. *Cell* **99**, 521–532 (1999).
27. Y. Aikawa, T. F. J. Martin, ARF6 regulates a plasma membrane pool of phosphatidylinositol (4, 5) bisphosphate required for regulated exocytosis. *J. Cell Biol.* **162**, 647–659 (2003).
28. A.-S. Bach *et al.*, ADP-ribosylation factor 6 regulates mammalian myoblast fusion through phospholipase D1 and phosphatidylinositol 4, 5-bisphosphate signaling pathways. *Mol. Biol. Cell* **21**, 2412–2424 (2010).
29. Y. Funakoshi, H. Hasegawa, Y. Kanaho, Activation mechanisms of PIP5K isozymes by the small GTPase ARF6. *Adv. Enzyme Regul.* **50**, 72–80 (2010).
30. K. Todorov-Völgyi *et al.*, Proteomics of mouse brain endothelium uncovers dysregulation of vesicular transport pathways during aging. *Nature Aging* **4**, 595–612 (2024).
31. A. Zellner *et al.*, CADASIL brain vessels show a HTRA1 loss-of-function profile. *Acta Neuropathol.* **136**, 111–125 (2018).
32. S. Ikeda *et al.*, Novel role of ARF6 in vascular endothelial growth factor-induced signaling and Angiogenesis. *Circ. Res.* **96**, 467–475 (2005).
33. T. Hongu *et al.*, Arf6 regulates tumour angiogenesis and growth through HGF-induced endothelial β1 integrin recycling. *Nat. Commun.* **6**, 7925 (2015).
34. C. T. Davis *et al.*, ARF6 inhibition stabilizes the vasculature and enhances survival during endotoxic shock. *J. Immunol.* **192**, 6045–6052 (2014).
35. M. T. Islam *et al.*, Endothelial-specific reduction in Arf6 impairs insulin-stimulated vasodilation and skeletal muscle blood flow resulting in systemic insulin resistance in mice. *Arterioscler. Thromb. Vasc. Biol.* **44**, 1101–1113 (2024).
36. C. R. Francis, M. L. Bell, M. M. Skripnichuk, E. J. Kushner, Arf6 is required for endocytosis and filamentous actin assembly during angiogenesis in vitro. *Microcirculation* **30**, e12831 (2023).
37. M. Vanlandewijck *et al.*, A molecular atlas of cell types and zonation in the brain vasculature. *Nature* **554**, 475–480 (2018).
38. L. He *et al.*, Single-cell RNA sequencing of mouse brain and lung vascular and vessel-associated cell types. *Sci. Data* **5**, 1–11 (2018).
39. Y.-K. Lee, H. Uchida, H. Smith, A. Ito, T. Sanchez, The isolation and molecular characterization of cerebral microvessels. *Nat. Protoc.* **14**, 3059–3081 (2019).
40. J. H. Yoo *et al.*, ARF6 is an actionable node that orchestrates oncogenic GNAQ signaling in uveal melanoma. *Cancer Cell* **29**, 889–904 (2016).
41. W. M. Bayliss, On the local reactions of the arterial wall to changes of internal pressure. *J. Physiol.* **28**, 220–231 (1902).
42. R. J. McCrimmon, B. M. Frier, Hypoglycaemia, the most feared complication of insulin therapy. *Diabete Metab.* **20**, 503–512 (1994).
43. X. Hu, T. M. De Silva, J. Chen, F. M. Faraci, Cerebral vascular disease and neurovascular injury in ischemic stroke. *Circ. Res.* **120**, 449–471 (2017).
44. L. Sokoloff, Energetics of functional activation in neural tissues. *Neurochem. Res.* **24**, 321–329 (1999).
45. D. Attwell *et al.*, Glial and neuronal control of brain blood flow. *Nature* **468**, 232–243 (2010).
46. B. H. Falkenburger, J. B. Jensen, B. Hille, Kinetics of PIP2 metabolism and KCNQ2/3 channel regulation studied with a voltage-sensitive phosphatase in living cells. *J. General Physiol.* **135**, 99–114 (2010).
47. R. A. Lacalle *et al.*, Type I phosphatidylinositol 4-phosphate 5-kinase homo- and heterodimerization determines its membrane localization and activity. *Faseb J.* **29**, 2371–2385 (2015).
48. M. Jarquin-Pardo, A. Fitzpatrick, F. J. Galiano, E. A. First, J. N. Davis, Phosphatidic acid regulates the affinity of the murine phosphatidylinositol 4-phosphate 5-kinase-Iβ for phosphatidylinositol-4-phosphate. *J. Cell. Biochem.* **100**, 112–128 (2007).
49. M. Krauss *et al.*, ARF6 stimulates clathrin/AP-2 recruitment to synaptic membranes by activating phosphatidylinositol phosphate kinase type Iγ. *J. Cell Biol.* **162**, 113–124 (2003).
50. S. D. Hansen, A. A. Lee, B. R. Duewell, J. T. Groves, Membrane-mediated dimerization potentiates PIP5K lipid kinase activity. *eLife* **11**, e73747 (2022).
51. P. Giguère *et al.*, ARF6 activation by Gαq signaling: Gαq forms molecular complexes with ARNO and ARF6. *Cell. Signal.* **18**, 1988–1994 (2006).
52. G. Laroche, P. M. Giguère, É. Dupré, G. Dupuis, J.-L. Parent, The N-terminal coiled-coil domain of the cytohesin/ARNO family of guanine nucleotide exchange factors interacts with Gαq. *Mol. Cell. Biochem.* **306**, 141–152 (2007).
53. X. J. Xǔ, C. S. Tong, M. Wu, Distinct impact of PI(4)P flux on PI(4,5)P2 steady states and oscillations. *Proc. Natl. Acad. Sci.* **123**, e2518354123 (2026).
54. W. Hilgemann Donald, R. Ball, Regulation of cardiac Na+, Ca2+ exchange and KATP potassium channels by PIP2. *Science* **273**, 956–959 (1996).
55. C. Z. Yang, H. Heimberg, C. D'Souza-Schorey, M. M. Mueckler, P. D. Stahl, Subcellular distribution and differential expression of endogenous ADP-ribosylation factor 6 in mammalian cells. *J. Biol. Chem.* **273**, 4006–4011 (1998).
56. M. Akiyama *et al.*, Tissue- and development-dependent expression of the small GTPase Arf6 in mice. *Dev. Dyn.* **239**, 3416–3435 (2010).
57. L. de la Cruz, C. Kushmerick, J. M. Sullivan, M. Kruse, O. Vivas, Hippocampal neurons maintain a large PtdIns(4)P pool that results in faster PtdIns(4,5)P2 synthesis. *J. General Physiol.* **154**, e202113001 (2022).

58. J. D. Horvath *et al.*, α-Synuclein-dependent increases in PIP5K1γ drive inositol signaling to promote neurotoxicity. *Cell Rep.* **42**, 113244 (2023).
59. R. Sannerud *et al.*, ADP ribosylation factor 6 (ARF6) controls amyloid precursor protein (APP) processing by mediating the endosomal sorting of BACE1. *Proc. Natl. Acad. Sci.* **108**, E559–E568 (2011).
60. R. Charles, Y. Namkung, M. Cotton, S. A. Laporte, A. Claing, β-Arrestin-mediated angiotensin II signaling controls the activation of ARF6 protein and endocytosis in migration of vascular smooth muscle cells. *J. Biol. Chem.* **291**, 3967–3981 (2016).
61. M. Nacke *et al.*, An ARF GTPase module promoting invasion and metastasis through regulating phosphoinositide metabolism. *Nat. Commun.* **12**, 1623 (2021).
62. W. Zhu *et al.*, Interleukin receptor activates a MYD88–ARNO–ARF6 cascade to disrupt vascular stability. *Nature* **492**, 252–255 (2012).
63. D. Kim, E. J. Cavanaugh, D. Simkin, Inhibition of transient receptor potential A1 channel by phosphatidylinositol-4, 5-bisphosphate. *Am. J. Physiol. Cell Physiol.* **295**, C92–C99 (2008).
64. A. M. Hashad, M. M. Abd-Alhaseeb, X. R. Lim, N. M. Mathieu, O. F. Harraz, PIP2 corrects an endothelial Piezo1 channelopathy. *Proc. Natl. Acad. Sci.* **122**, e2522750122 (2025).
65. M. Félétou, Y. Huang, P. M. Vanhoutte, Endothelium-mediated control of vascular tone: COX-1 and COX-2 products. *British J. Pharmacol.* **164**, 894–912 (2011).
66. L. de la Cruz, R. Riquelme, O. Vivas, A. Barria, J. B. Jensen, Dishevelled coordinates phosphoinositide kinases PI4KIIIα and PIP5KIγ for efficient PtdInsP2 synthesis. *J. Cell Sci.* **135**, jcs259145 (2022).
67. S. Earley, D. Kleinfeld, PIP2 as the "coin of the realm" for neurovascular coupling. *Proc. Natl. Acad. Sci.* **118**, e2106308118 (2021).